



UNIVERSITY OF LEEDS

This is a repository copy of *The method of fundamental solutions for Brinkman flows. Part I. Exterior domains.*

White Rose Research Online URL for this paper:  
<https://eprints.whiterose.ac.uk/168747/>

Version: Accepted Version

---

**Article:**

Karageorghis, A, Lesnic, D [orcid.org/0000-0003-3025-2770](https://orcid.org/0000-0003-3025-2770) and Marin, L (2021) The method of fundamental solutions for Brinkman flows. Part I. Exterior domains. *Journal of Engineering Mathematics*, 126. 10. ISSN 0022-0833

<https://doi.org/10.1007/s10665-020-10082-3>

---

© The Author(s), under exclusive licence to Springer Nature B.V. part of Springer Nature 2021. This is an author produced version of an article published in *Journal of Engineering Mathematics*. Uploaded in accordance with the publisher's self-archiving policy.

**Reuse**

Items deposited in White Rose Research Online are protected by copyright, with all rights reserved unless indicated otherwise. They may be downloaded and/or printed for private study, or other acts as permitted by national copyright laws. The publisher or other rights holders may allow further reproduction and re-use of the full text version. This is indicated by the licence information on the White Rose Research Online record for the item.

**Takedown**

If you consider content in White Rose Research Online to be in breach of UK law, please notify us by emailing [eprints@whiterose.ac.uk](mailto:eprints@whiterose.ac.uk) including the URL of the record and the reason for the withdrawal request.



[eprints@whiterose.ac.uk](mailto:eprints@whiterose.ac.uk)  
<https://eprints.whiterose.ac.uk/>

# THE METHOD OF FUNDAMENTAL SOLUTIONS FOR BRINKMAN FLOWS. PART I. EXTERIOR DOMAINS

ANDREAS KARAGEORGHIS, DANIEL LESNIC, AND LIVIU MARIN

ABSTRACT. The method of fundamental solutions (MFS) is developed for solving numerically the Brinkman flow in the porous medium outside obstacles of known or unknown shapes. The MFS uses the fundamental solution of the Brinkman equation as in the boundary element method (BEM), but the single-layer representation is desingularised by moving the boundary sources to fictitious points outside the solution domain. In the case of unbounded flow past obstacles, these source points are placed in the domain inside the obstacle on a contracted fictitious pseudo-boundary. When the obstacle is known, then the fluid flow in porous media problem is direct, linear and well-posed. In the case of Brinkman flow in the porous medium outside an infinitely long circular cylinder, the MFS numerical solution is found to be in very good agreement with the available analytical solution. However, when the obstacle is unknown and has to be determined from fluid velocity measurements at some points inside the fluid, the resulting problem becomes inverse, non-linear and ill-posed. The MATLAB<sup>©</sup> optimization toolbox routine `lsqnonlin` is employed for minimizing the least-squares gap between the computed and measured fluid velocity which is further penalised with extra smoothness regularization terms in order to overcome the instability of the solution. For proper choices of the regularization parameters involved, accurate and stable numerical reconstructions are achieved for various star-shaped obstacles.

## 1. INTRODUCTION

The Brinkman equation was introduced to mitigate in between the microscopic and macroscopic scales/levels represented by the Stokes's and Darcy's equations, respectively, for the steady-state viscous flow through a porous medium, [4]. Since its discovery, this equation has been found appropriate to model various practical applications in petroleum engineering, [15] and biological flows related to biofilms, [6], blood clots, [13] and flagellar motion in gels, [14].

The Brinkman viscous incompressible fluid flow in a porous medium outside a two-dimensional bounded obstacle  $\Omega \subset \mathbb{R}^2$  is governed by the Brinkman equation, see e.g. [5, 19],

$$\Delta \mathbf{v} - \frac{1}{\mu} \nabla p - \kappa^2 \mathbf{v} = \mathbf{0} \quad \text{in } \mathbb{R}^2 \setminus \overline{\Omega}, \quad (\text{where } \overline{\Omega} \text{ denotes the closure of } \Omega) \quad (1.1)$$

along with the continuity equation for incompressible flows

$$\nabla \cdot \mathbf{v} = 0 \quad \text{in } \mathbb{R}^2 \setminus \overline{\Omega}, \quad (1.2)$$

---

*Date:* October 11, 2020.

*2010 Mathematics Subject Classification.* Primary 65N35; Secondary 65N21, 65N38.

*Key words and phrases.* Brinkman flow; method of fundamental solutions; inverse problem; nonlinear minimization.

where  $\mathbf{v}$  is the fluid velocity,  $p$  is the pressure,  $\mu$  is the dynamic viscosity of the fluid, and  $\kappa^2 > 0$  represents the resistivity of the porous medium to the flow (or the reciprocal of the permeability). For simplicity, the body forces have been assumed absent and the boundary  $\partial\Omega$  is assumed sufficiently smooth, e.g. of class  $C^2$ . The Brinkman equation (1.1) can be obtained formally by seeking a solution  $\mathbf{V}(\mathbf{x}, t)$  of the time-dependent Stokes equations

$$\varrho \frac{\partial \mathbf{V}}{\partial t} = \mu \Delta \mathbf{V} - \nabla p,$$

where  $\varrho$  is the fluid density, in the Laplace transform form  $\mathbf{V}(\mathbf{x}, t) = \mathbf{v}(\mathbf{x}) e^{st}$ , where  $\kappa^2 = \varrho s / \mu$ .

For  $\kappa = 0$ , the Brinkman equation (1.1) becomes the steady-state Stokes equation governing slow viscous fluid flow. However, the solution of the Brinkman equation do not approach the corresponding solution of the Stokes equation as  $\kappa \searrow 0$ , [16]. In particular, for any  $\kappa > 0$ , the Brinkman model regularizes the two-dimensional Stokes flow (with  $\kappa = 0$ ) to overcome the Stokes paradox (logarithmic growth of the fluid velocity at large distances), [16]. Therefore, the MFS analysis of the current study based on the fundamental solution of the Brinkman equation (1.1) (and the continuity equation (1.2)) is different from that for the Stokes equation, see [1, 22].

Associated with (1.1) and (1.2) are the boundary no-slip condition

$$\mathbf{v} = \mathbf{0} \quad \text{on} \quad \partial\Omega \tag{1.3}$$

and the infinity conditions for ambient flow with uniform fluid flow velocity  $\mathbf{U}^\infty$  given by

$$\lim_{|\mathbf{x}| \rightarrow \infty} (\mathbf{v}(\mathbf{x}) - \mathbf{U}^\infty) = \mathbf{0} \tag{1.4}$$

and

$$\lim_{|\mathbf{x}| \rightarrow \infty} (p(\mathbf{x}) + \mu \kappa^2 \mathbf{U}^\infty \cdot \mathbf{x}) = \text{finite constant} =: c. \tag{1.5}$$

In order to accommodate these infinity conditions, we introduce the perturbed fluid velocity  $\mathbf{u}$  and pressure  $p$  given by

$$\mathbf{u}(\mathbf{x}) = \mathbf{v}(\mathbf{x}) - \mathbf{U}^\infty, \quad p(\mathbf{x}) = p(\mathbf{x}) + \mu \kappa^2 \mathbf{U}^\infty \cdot \mathbf{x}, \tag{1.6}$$

which satisfy the following problem:

$$\Delta \mathbf{u} - \frac{1}{\mu} \nabla p - \kappa^2 \mathbf{u} = \mathbf{0} \quad \text{in} \quad \mathbb{R}^2 \setminus \bar{\Omega}, \tag{1.7}$$

$$\nabla \cdot \mathbf{u} = 0 \quad \text{in} \quad \mathbb{R}^2 \setminus \bar{\Omega}, \tag{1.8}$$

$$\mathbf{u} = -\mathbf{U}^\infty \quad \text{on} \quad \partial\Omega, \tag{1.9}$$

$$\lim_{|\mathbf{x}| \rightarrow \infty} \mathbf{u}(\mathbf{x}) = \mathbf{0}, \tag{1.10}$$

$$\lim_{|\mathbf{x}| \rightarrow \infty} p(\mathbf{x}) = c. \tag{1.11}$$

The analysis for the Brinkman flow model (1.1)–(1.5) or (1.7)–(1.11) (also called the Stokes resolvent) has been carried out in [3, 21, 10]. It should be mentioned that in these studies the imposed infinity conditions, namely,

$$(|\mathbf{u}||\nabla\mathbf{u}|)(\mathbf{x}) = o(|\mathbf{x}|^{-1}), \quad (|\mathbf{u}||p|)(\mathbf{x}) = o(|\mathbf{x}|^{-1}), \quad \text{as } |\mathbf{x}| \rightarrow \infty, \quad (1.12)$$

are nonlinear and the uniqueness of a classical solution

$$(\mathbf{u}, p) \in (C^2(\mathbb{R}^2 \setminus \overline{\Omega}) \cap C(\mathbb{R}^2 \setminus \Omega)) \times C^1(\mathbb{R}^2 \setminus \overline{\Omega})$$

does not follow directly. In (1.12),  $\nabla\mathbf{u}$  represents the perturbation velocity gradient tensor having

the components  $(\partial_{x_i} u_j)_{i,j=1,2}$ . The norm of this vector is defined as  $|\nabla\mathbf{u}| = \sqrt{\sum_{i,j=1}^2 (\partial_{x_i} u_j)^2}$ .

However, uniqueness can be assured if we require the infinity conditions (1.10) and (1.11) to be satisfied in the form

$$|\mathbf{u}(\mathbf{x})| = o(|\mathbf{x}|^{-1}), \quad |\nabla\mathbf{u}(\mathbf{x})| = O(1), \quad |p(\mathbf{x})| = O(1), \quad \text{as } |\mathbf{x}| \rightarrow \infty. \quad (1.13)$$

In the next section, we introduce the method of fundamental solutions (MFS) [8] for the solution of the Brinkman flow model (1.7)–(1.11).

## 2. THE METHOD OF FUNDAMENTAL SOLUTIONS (MFS)

The MFS for interior Brinkman flows was developed in [17, 20]. In this paper, we propose the MFS formulation for exterior Brinkman flows in unbounded domains.

The fundamental solution of the Brinkman equations (1.1) and (1.2) (or (1.7) and (1.8)) in two dimensions is given by, [20],

$$G_{ik}(\mathbf{x}, \mathbf{x}') = \frac{1}{2\pi\mu\kappa^2|\mathbf{x} - \mathbf{x}'|^2} \left[ (-1 + \kappa|\mathbf{x} - \mathbf{x}'|K_1(\kappa|\mathbf{x} - \mathbf{x}'|) + \kappa^2|\mathbf{x} - \mathbf{x}'|^2K_0(\kappa|\mathbf{x} - \mathbf{x}'|)) \delta_{ik} \right. \\ \left. + \frac{(x_i - x'_i)(x_k - x'_k)}{|\mathbf{x} - \mathbf{x}'|^2} (2 - \kappa^2|\mathbf{x} - \mathbf{x}'|^2K_2(\kappa|\mathbf{x} - \mathbf{x}'|)) \right], \quad i, k = 1, 2, \quad (2.1)$$

$$P_k(\mathbf{x}, \mathbf{x}') = \frac{x_k - x'_k}{2\pi|\mathbf{x} - \mathbf{x}'|^2}, \quad k = 1, 2, \quad (2.2)$$

where  $\mathbf{x} = (x_1, x_2)$ ,  $\mathbf{x}' = (x'_1, x'_2)$ ,  $\mathbf{I} = (\delta_{ik})_{i,k=1,2}$  is the identity matrix (or the Kronecker delta tensor), and  $K_n$  is the modified Bessel function of the second kind of order  $n$ .

Using that

$$\frac{2K_1(x)}{x} = K_2(x) - K_0(x),$$

we can rewrite (2.1) in the equivalent form

$$G_{ik}(\mathbf{x}, \mathbf{x}') = \frac{1}{2\pi\mu} \left[ \left( -\frac{1}{\kappa^2|\mathbf{x} - \mathbf{x}'|^2} + \frac{K_0(\kappa|\mathbf{x} - \mathbf{x}'|) + K_2(\kappa|\mathbf{x} - \mathbf{x}'|)}{2} \right) \delta_{ik} \right.$$

$$+ \frac{(x_i - x'_i)(x_k - x'_k)}{|\mathbf{x} - \mathbf{x}'|^2} \left( \frac{2}{\kappa^2 |\mathbf{x} - \mathbf{x}'|^2} - K_2(\kappa |\mathbf{x} - \mathbf{x}'|) \right) \Big], \quad i, k = 1, 2, \quad (2.3)$$

present in other references, e.g. [11] and [16].

Justified by the density results established in [17], using (2.1) and (2.2), in the MFS we seek an approximate solution for the perturbed fluid velocity  $\mathbf{u} = (u_1, u_2)$  satisfying (1.7) and (1.8) in the form

$$u_i(\mathbf{x}) = \sum_{j=1}^N [\alpha_j G_{i1}(\mathbf{x}, \boldsymbol{\xi}_j) + \beta_j G_{i2}(\mathbf{x}, \boldsymbol{\xi}_j)], \quad \mathbf{x} \in \mathbb{R}^2 \setminus \Omega, \quad i = 1, 2, \quad (2.4)$$

where  $\boldsymbol{\xi}_j$  for  $j = \overline{1, N}$  are the source points situated outside the solution domain  $\mathbb{R}^2 \setminus \Omega$ , i.e. in  $\Omega$ , for example lying on a contracted pseudo-boundary  $\partial\Omega' \subset \Omega$  (e.g., if  $\Omega$  is a star-shaped domain parameterised by a polar radius  $r(\theta)$ , see later on (4.3), then we choose  $\Omega' \subset \Omega$  as a contracted star-shaped sub-domain parameterised by a polar radius that is a sub-unitary fraction  $\eta \in (0, 1)$  of  $r(\theta)$ ). (Note also that throughout the paper, the notation  $j = \overline{1, N}$  denotes  $j = 1, 2, \dots, N$ .) Remark that since

$$\lim_{|\mathbf{x} - \mathbf{x}'| \rightarrow \infty} K_0(\kappa |\mathbf{x} - \mathbf{x}'|) = \lim_{|\mathbf{x} - \mathbf{x}'| \rightarrow \infty} K_2(\kappa |\mathbf{x} - \mathbf{x}'|) = 0,$$

from (2.1), the infinity condition (1.10) is also justified by the function defined in (2.4) via (2.3). Also, since  $\mathbf{x} \in \mathbb{R}^2 \setminus \Omega$  and  $(\boldsymbol{\xi}_j)_{j=\overline{1, N}} \in \Omega$  belong to disjoint sets, the fundamental solutions  $G_{i1}(\mathbf{x}, \boldsymbol{\xi}_j)$  and  $G_{i2}(\mathbf{x}, \boldsymbol{\xi}_j)$  for  $i = 1, 2$  and  $j = \overline{1, N}$  are never singular, and (2.4) and (2.6) below satisfy automatically the Brinkman and continuity equations (1.7) and (1.8). Consequently, we do not have to discretise these partial differential equations. Instead, we only need to determine the unknown real coefficients  $\boldsymbol{\alpha} = (\alpha_j)_{j=\overline{1, N}}$  and  $\boldsymbol{\beta} = (\beta_j)_{j=\overline{1, N}}$ , we collocate the boundary condition (1.9) at  $M \geq N$  distinct points  $(\mathbf{x}_k)_{k=\overline{1, M}}$  on  $\partial\Omega$ , namely,

$$\sum_{j=1}^N [\alpha_j G_{i1}(\mathbf{x}_k, \boldsymbol{\xi}_j) + \beta_j G_{i2}(\mathbf{x}_k, \boldsymbol{\xi}_j)] = -U_i^\infty, \quad i = 1, 2, \quad k = \overline{1, M}, \quad (2.5)$$

where  $\mathbf{U}^\infty = (U_1^\infty, U_2^\infty)$ .

Expression (2.5) represents a system of  $2M$  linear equations in the  $2N$  unknown coefficients  $\boldsymbol{\alpha}$  and  $\boldsymbol{\beta}$ , which can be solved using an ordinary least-squares method. Once the coefficients  $\boldsymbol{\alpha}$  and  $\boldsymbol{\beta}$  have been determined, the perturbation fluid velocity  $\mathbf{u}$  can be obtained explicitly at any point  $\mathbf{x}$  inside the fluid domain  $\mathbb{R}^2 \setminus \overline{\Omega}$  from equation (2.4). The fluid pressure can also be obtained (up to an arbitrary constant  $c$ ) from

$$p(\mathbf{x}) = c + \sum_{j=1}^N [\alpha_j P_1(\mathbf{x}, \boldsymbol{\xi}_j) + \beta_j P_2(\mathbf{x}, \boldsymbol{\xi}_j)], \quad \mathbf{x} \in \mathbb{R}^2 \setminus \Omega. \quad (2.6)$$

## 3. NUMERICAL EXAMPLE FOR THE DIRECT PROBLEM

We consider the Brinkman fluid flow in a porous medium outside an infinitely long circular cylinder of radius  $a > 0$  centred at the origin, i.e. outside the disk  $\Omega = \{\mathbf{x} \in \mathbb{R}^2; |\mathbf{x}| < a\}$ ; placed in a uniform flow of velocity  $\mathbf{U}^\infty$ , whose analytical solution for the perturbed fluid velocity and pressure (up to a constant) are given by, see e.g. [14, 17],

$$\begin{aligned} \mathbf{u}(\mathbf{x}) &= \frac{\mathbf{U}^\infty}{K_0(\kappa a)} \left[ \frac{a^2}{|\mathbf{x}|^2} K_2(\kappa a) - K_2(\kappa|\mathbf{x}|) - K_0(\kappa|\mathbf{x}|) \right] \\ &+ \frac{2(\mathbf{U}^\infty \cdot \mathbf{x}) \mathbf{x}}{K_0(\kappa a) |\mathbf{x}|^2} \left[ K_2(\kappa|\mathbf{x}|) - \frac{a^2}{|\mathbf{x}|^2} K_2(\kappa a) \right], \quad \mathbf{x} \in \mathbb{R}^2 \setminus \Omega, \end{aligned} \quad (3.1)$$

$$p(\mathbf{x}) = -\frac{\mu \kappa^2 a^2 K_2(\kappa a) (\mathbf{U}^\infty \cdot \mathbf{x})}{K_0(\kappa a) |\mathbf{x}|^2}, \quad \mathbf{x} \in \mathbb{R}^2 \setminus \Omega. \quad (3.2)$$

The source and collocation points  $(\boldsymbol{\xi}_j)_{j=1, \overline{N}}$  and  $(\mathbf{x}_k)_{k=1, \overline{M}}$  were spread uniformly on a contracted circle  $\partial\Omega'$  (of radius  $\eta a$  with  $\eta \in (0, 1)$ ) and the circle  $\partial\Omega$  (of radius  $a$ ), respectively. In the numerical experiments we took  $\mu = 1$ ,  $a = 1$ ,  $\kappa = 1$  and  $\mathbf{U}^\infty = (U^\infty, 0) = (1, 0)$ . In Table 1 we present the maximum absolute errors obtained at 660 radially uniformly distributed points in the annulus  $\{1 \leq |\mathbf{x}| \leq 2\} \subset \mathbb{R}^2 \setminus \Omega$  for the perturbed velocity and pressure for various values of  $M, N$  and  $\eta = 0.8$  (noting that the accuracy of the numerical results was not significantly affected by any reasonable choice of  $\eta \in (0, 1)$  which is neither too small or too close to unity). Clearly, as the number of degrees of freedom increases, the MFS approximate solutions converge to the exact solutions. In Figure 1 we present the maximum errors obtained at 101 uniformly distributed points on circles of radii  $d = 1 + (\ell - 1)0.1$ ,  $\ell = \overline{1, 11}$ . From this figure we observe that the error decreases as we move away from the boundary  $\partial\Omega$ . We also calculated the errors at 101 uniformly distributed points on the circle of radius  $d = 1.1$  for different numbers of degrees of freedom. The corresponding plots depicting the variation of the errors are shown in Figure 2. From this figure we observe that, in contrast to the errors in velocities, the error in pressure oscillates a lot around the circular contour, but it is still bounded and decreases to zero as the numbers of degrees of freedom increase. In Figure 3 we present the fluid velocity vector  $\mathbf{v}(\mathbf{x}) = \mathbf{u}(\mathbf{x}) + \mathbf{U}^\infty$  and the pressure contours  $p(\mathbf{x}) = p(\mathbf{x}) - \mu \kappa^2 (\mathbf{U}^\infty \cdot \mathbf{x})$  obtained using the MFS with  $M = 192$ ,  $N = 144$  and  $\eta = 0.8$ . Excellent agreement with the corresponding analytical solutions derived from (3.1) and (3.2) is reported. Finally, we calculated the maximum absolute errors obtained at 660 radially uniformly distributed points in the annulus  $\{1 \leq |\mathbf{x}| \leq 2\} \subset \mathbb{R}^2 \setminus \Omega$  for the perturbed velocity and pressure for  $M = 192, N = 144$  when varying the parameters  $a, \kappa, \mu$  and  $U^\infty$ . As observed in Table 2, there is only a very slight decrease in accuracy when we increase the values of these parameters.

TABLE 1. Maximum absolute errors in perturbed velocity  $\mathbf{u} = (u_1, u_2)$  and pressure ( $E(u_1)$ ,  $E(u_2)$  and  $E(p)$ , respectively) for different numbers of degrees of freedom

$M$	$N$	$E(u_1)$	$E(u_2)$	$E(p)$
24	18	1.5997(-2)	2.3089(-2)	2.5544(-1)
48	36	2.8017(-4)	2.3380(-4)	3.6695(-3)
96	72	1.0418(-7)	8.8276(-8)	4.5182(-6)
192	144	1.2657(-14)	1.4128(-14)	1.4628(-12)

TABLE 2. Maximum absolute errors in perturbed velocity  $\mathbf{u} = (u_1, u_2)$  and pressure ( $E(u_1)$ ,  $E(u_2)$  and  $E(p)$ , respectively) for  $M = 192$ ,  $N = 144$  obtained when varying the parameters  $a, \kappa, \mu$  and  $U^\infty$

$a$	$\kappa$	$\mu$	$U^\infty$	$E(u_1)$	$E(u_2)$	$E(p)$
1	1	1	1	1.2657(-14)	1.4128(-14)	1.4628(-12)
5	1	1	1	1.2124(-13)	1.3209(-13)	2.6255(-12)
10	1	1	1	5.7021(-13)	6.8523(-13)	7.2538(-12)
1	5	1	1	1.2168(-13)	1.3211(-13)	1.3167(-11)
1	10	1	1	5.8509(-13)	6.9268(-13)	7.3378(-11)
1	1	5	1	1.1435(-14)	1.4794(-14)	7.3306(-12)
1	1	10	1	1.1435(-14)	1.4794(-14)	1.4661(-11)
1	1	1	5	6.2172(-14)	7.1165(-14)	7.2804(-12)
1	1	1	10	1.2434(-13)	1.4233(-13)	1.4561(-11)

#### 4. INVERSE OBSTACLE PROBLEM

In this section we investigate the identification of an unknown simply-connected bounded planar obstacle  $\Omega$  immersed in a Brinkman flow of incompressible fluid from the fluid velocity measurement

$$\mathbf{v} = \mathbf{\Phi} \quad \text{on} \quad \Gamma, \quad (4.1)$$

or

$$\mathbf{u} = \boldsymbol{\varphi} \quad \text{on} \quad \Gamma, \quad (4.2)$$

where  $\boldsymbol{\varphi} = \mathbf{\Phi} - \mathbf{U}^\infty$  and  $\Gamma \subset \mathbb{R}^2 \setminus \overline{\Omega}$  is an arc placed outside the obstacle  $\Omega$ . Here the arc  $\Gamma$  is understood as a connected open subset of a simple closed analytic curve  $\tilde{\Gamma}$  containing  $\overline{\Omega}$  in its interior.

**Uniqueness Theorem.** *Assume that  $\Omega_1$  and  $\Omega_2$  are two simply-connected bounded obstacles (with sufficiently smooth boundaries, e.g. of class  $C^2$ ) contained in the interior of  $\tilde{\Gamma}$ . Let  $\mathbf{v}_1$  and  $\mathbf{v}_2$  be the solutions for the fluid velocity satisfying (1.1)–(1.5) corresponding to the obstacles  $\Omega_1$  and  $\Omega_2$ , respectively. If  $\mathbf{v}_1$  and  $\mathbf{v}_2$  coincide with a given  $\mathbf{\Phi}$  on  $\Gamma$ , as defined in (4.1), then  $\Omega_1 = \Omega_2$ .*

**Proof.** Some parts of the proof follow [12] for the corresponding Oseen flow inverse problem. From the representation of the solution as a single-layer potential it can be seen that  $\mathbf{v}_1$  and  $\mathbf{v}_2$  are analytic in  $\mathbb{R}^2 \setminus \overline{\Omega}_1$  and  $\mathbb{R}^2 \setminus \overline{\Omega}_2$ , respectively. Then, from the unique continuation principle it follows that  $\mathbf{v}_1 = \mathbf{v}_2 = \Phi$  on  $\Gamma$  implies that  $\mathbf{v}_1 = \mathbf{v}_2$  on  $\tilde{\Gamma}$ . By solving the direct well-posed problem for  $(\mathbf{v}_1 - \mathbf{v}_2)$  in the exterior domain  $\mathbb{R}^2 \setminus \tilde{\Omega}$  of the domain  $\tilde{\Omega}$  with boundary  $\tilde{\Gamma}$ , we also get that  $\mathbf{v}_1 = \mathbf{v}_2$  in  $\mathbb{R}^2 \setminus \tilde{\Omega}$ . By analyticity, we obtain that  $\mathbf{v}_1 = \mathbf{v}_2$  in  $\mathbb{R}^2 \setminus (\Omega_1 \cup \Omega_2) =: D$ . If  $\Omega_1 \neq \Omega_2$ , then we can assume that the bounded domain  $\Omega^* := \overline{\Omega}_1 \cup \overline{\Omega}_2 \setminus \overline{\Omega}_2$  is non-empty (and measurable). Then  $\mathbf{v} := \mathbf{v}_2$  defined in  $\Omega^*$  satisfies (1.1), (1.2) and  $\mathbf{v} = \mathbf{0}$  on  $\partial\Omega^*$ . This is because on the portion of  $\partial\Omega^*$  that belongs to  $\partial\Omega_1$  but not to  $\partial\Omega_2$  we have that  $\mathbf{v} = \mathbf{v}_1 = \mathbf{v}_2 = \mathbf{0}$ , whilst on the remaining portion of  $\partial\Omega^*$  that belongs to  $\partial\Omega_2$  we have that  $\mathbf{v} = \mathbf{v}_2 = \mathbf{0}$ . Then, from the uniqueness of solution of the interior problem for Brinkman's and divergence equations (1.1) and (1.2) in the bounded domain  $\Omega^*$  with homogeneous boundary condition  $\mathbf{v} = \mathbf{0}$  on  $\partial\Omega^*$ , [10], it follows that  $\mathbf{v} = \mathbf{0}$  in  $\Omega^* \subset \mathbb{R}^2 \setminus \Omega_2$ . From this and the analyticity of the function  $\mathbf{v}_2$  in  $\mathbb{R}^2 \setminus \overline{\Omega}_2$  we obtain that  $\mathbf{v}_2 = \mathbf{0}$  in  $\mathbb{R}^2 \setminus \Omega_2$ . This is in contradiction with the infinity condition (1.4) with  $\mathbf{U}^\infty \neq \mathbf{0}$ . This implies that  $\Omega^*$  cannot be non-empty, i.e.  $\Omega^* = \emptyset$  and thus  $\Omega_1 \subset \Omega_2$ . A similar analysis for the domain  $\Omega^* := \overline{\Omega}_1 \cup \overline{\Omega}_2 \setminus \overline{\Omega}_1$  yields that  $\Omega_2 \subset \Omega_1$ . Therefore,  $\Omega_1 = \Omega_2$  which concludes the uniqueness proof.  $\square$

In terms of the perturbations  $\mathbf{u}$  and  $p$ , the inverse problem requires solving for the unknown triplet  $(\mathbf{u}, p, \Omega)$  satisfying (1.7)–(1.11) and (4.2). This problem and its MFS combined nonlinear minimization is similar to that previously treated in [7] for Oseen flow. We assume that  $\Omega$  is star-shaped with respect to the origin, parametrised by the radial polar coordinate  $r(\vartheta) \in (0, r_{\max}]$  for  $\vartheta \in [0, 2\pi)$ , where  $r_{\max} > 0$  is an *a priori* known upper bound of the size of the obstacle, namely,

$$\Omega = \{r(\vartheta) (\cos \vartheta, \sin \vartheta) \mid \vartheta \in [0, 2\pi)\}. \quad (4.3)$$

Taking, for simplicity,  $M = N$  we impose the no-slip boundary condition (1.9) at the points  $\mathbf{x}_i = (r_i \cos \vartheta_i, r_i \sin \vartheta_i)$  where  $r_i := r(\vartheta_i)$ ,  $\vartheta_i = 2\pi(i-1)/N$  for  $i = \overline{1, N}$ . We also choose the corresponding sources  $\boldsymbol{\xi}_j = \eta \mathbf{x}_j$  for  $j = \overline{1, N}$ , where  $\eta \in (0, 1)$  is a contraction factor to be determined. Since  $\mathbf{r} = (r_i)_{i=\overline{1, N}}$  is unknown in the inverse geometric problem, we impose the extra information (4.2) at  $L$  uniformly distributed points  $(\mathbf{x}_{N+\ell})_{\ell=\overline{1, L}}$  on  $\Gamma$ . The resulting nonlinear regularized least-squares functional that needs to be minimized takes the following form:

$$\begin{aligned} T_{\lambda_1, \lambda_2}(\boldsymbol{\alpha}, \boldsymbol{\beta}, \mathbf{r}, \eta) &:= \sum_{k=1}^2 \sum_{i=1}^N \left\{ \sum_{j=1}^N [\alpha_j G_{k1}(\mathbf{x}_i, \boldsymbol{\xi}_j) + \beta_j G_{k2}(\mathbf{x}_i, \boldsymbol{\xi}_j)] + U_k^\infty \right\}^2 \\ &+ \sum_{k=1}^2 \sum_{\ell=1}^L \left\{ \sum_{j=1}^N [\alpha_j G_{k1}(\mathbf{x}_{N+\ell}, \boldsymbol{\xi}_j) + \beta_j G_{k2}(\mathbf{x}_{N+\ell}, \boldsymbol{\xi}_j)] - \varphi_k(\mathbf{x}_{N+\ell}) \right\}^2 \\ &+ \lambda_1 \sum_{j=1}^N (\alpha_j^2 + \beta_j^2) + \lambda_2 \sum_{i=2}^N (r_i - r_{i-1})^2, \end{aligned} \quad (4.4)$$

where  $\lambda_1 \geq 0$  and  $\lambda_2 \geq 0$  are regularization parameters penalizing the MFS spectral representation (2.4) and the first order smoothness of the boundary  $\partial\Omega$  of the unknown obstacle  $\Omega$ , respectively. The minimization of (4.4) subject to the simple bounds on the variables

$$\begin{aligned} -10^5 \leq \alpha_j \leq 10^5, \quad -10^5 \leq \beta_j \leq 10^5, \quad j = \overline{1, N}, \\ 10^{-5} \leq r_i \leq r_{\max}, \quad i = \overline{1, N}, \quad \text{and} \quad 0.1 \leq \eta \leq 0.99, \end{aligned} \quad (4.5)$$

is performed using the MATLAB<sup>©</sup> optimization toolbox routine `lsqnonlin` [18] based on the subspace trust region method. The minimization process starts with an initial guess for the  $(3N + 1)$  unknowns in the feasible set (4.5) and continues to iterate until one of the following criteria is satisfied:

- the maximum number of iterations (`MaxIter`) is reached;
- the maximum number of function evaluations (`MaxFunEvals`) of the objective function (4.4) is reached;
- the termination tolerance for the solution  $\mathbf{X} = (\boldsymbol{\alpha}, \boldsymbol{\beta}, \mathbf{r}, \eta)$  (`TolX`) or for the objective function  $T_{\lambda_1, \lambda_2}(\mathbf{X})$  (`TolFun`) is achieved.

As previously experienced with other minimization studies, see e.g. [9, 7], we took `MaxFunEvals` =  $2 \times 10^6$ , `TolX` = `TolFun` =  $10^{-14}$  and controlled the convergence of (4.4) with appropriate values of `MaxIter`. In most cases, the iterative process was ceased when `MaxIter` was exhausted, but in some instances the tolerance `TolX` was reached.

## 5. NUMERICAL RESULTS AND DISCUSSION FOR THE INVERSE OBSTACLE PROBLEM

In all the following examples, we choose the location of the measurement curve  $\Gamma$  to be a circle of radius  $R_1 = 2.5$  (centred at the origin), which is neither too close nor too far from the unity, which represents a characteristic dimension of the obstacles to be retrieved.

For the Brinkman flow, we took the parameters  $\mu = 1$ ,  $\kappa = 1$  and  $\mathbf{U}^\infty = (U^\infty, 0) = (1, 0)$ . In all numerical experiments we took  $r_{\max} = 1.5$ . In order to simulate the errors that are inherently present in any practical measurement and to test the stability of the inversion, the measured data (4.2) is perturbed by a multiplicative noise as

$$\boldsymbol{\varphi}^\varepsilon(\mathbf{x}_{\ell+N}) = (1 + \chi \zeta) \boldsymbol{\varphi}(\mathbf{x}_{\ell+N}), \quad \ell = \overline{1, L}, \quad (5.1)$$

where  $\zeta$  represents the percentage of noise and  $\chi$  is a pseudo-random noisy variable drawn from a uniform distribution in  $[-1, 1]$  using the MATLAB<sup>©</sup> command `-1 + 2*rand(1,L)`. When the noisy data (5.1) is inverted, due to the ill-posedness of the inverse obstacle problem, regularization needs to be employed in the functional (4.4). In this study we choose the regularization parameters  $\lambda_1$  and  $\lambda_2$  by taking one to be zero and varying the other by trial and error or by the L-curve analysis, [7, 9]. In all examples considered we took  $M = N = 20$ ,  $L = 51$  and the initial guesses  $\boldsymbol{\alpha}^0 = \boldsymbol{\beta}^0 = \mathbf{0}$  and  $\eta^0 = 2/3$ .

**5.1. Example 1: Circular obstacle.** In this case the obstacle to be reconstructed is a circle of radius

$$r(\vartheta) = 1, \quad \vartheta \in [0, 2\pi). \quad (5.2)$$

The input perturbed velocity data (4.2) were constructed from the exact solution (3.1). We took the initial guess  $\mathbf{r}^0 = 0.7$ . In Figure 4(a), the convergence of results obtained with no noise and no regularization for different numbers of iterations `niter` is illustrated. In Figures 4(b) and 4(c) we present the plots of the reconstructed boundary for various values of the regularization parameter  $\lambda_1$  when  $\lambda_2 = 0$ , and  $\lambda_2$  when  $\lambda_1 = 0$ , respectively, and  $\zeta = 5\%$  after 1000 iterations. From these figures it can be seen that regularization with  $\lambda_2$ , which penalizes the smoothness of the shape to be reconstructed, is more important than the regularization with  $\lambda_1$  which is imposed to alleviate the ill-conditioning of the MFS.

**5.2. Example 2: Bean-shaped obstacle.** We next consider the bean-shaped domain [2, 7, 12] with polar radius

$$r(\vartheta) = \frac{1 + 0.9 \cos(\vartheta) + 0.1 \sin(\vartheta)}{1 + 0.75 \cos(\vartheta)}, \quad \vartheta \in [0, 2\pi). \quad (5.3)$$

We took the initial guess  $\mathbf{r}^0 = 1$ . The input velocity data (4.2) is numerically simulated by first solving the corresponding direct problem with  $M = 192$  and  $N = 144$ . In Figure 5(a) we present the results obtained with no noise and no regularization for different numbers of iterations `niter`. Compared to the smooth circular obstacle (5.2) of the previous example, the bean-shaped domain (5.3) presents a cusp facing the incoming flow which makes the convergence of its reconstruction much slower needing more than around 10000 iterations. In Figures 5(b) and 5(c) we present the plots of the reconstructed boundary for various values of the regularization parameter  $\lambda_1$  when  $\lambda_2 = 0$ , and  $\lambda_2$  when  $\lambda_1 = 0$ , respectively, and  $\zeta = 5\%$  after 1000 iterations. Unlike in the previous smooth circular example where regularization with  $\lambda_2$  (and  $\lambda_1 = 0$ ) produced slightly better reconstructions than regularization with  $\lambda_1$  (and  $\lambda_2 = 0$ ), in this example the regularization with either  $\lambda_1$  or  $\lambda_2$  yields similar results in terms of accuracy and stability of the bean-shape reconstruction.

**5.3. Example 6: Peanut-shaped obstacle.** We finally consider the peanut-shaped domain [7, 12] described by

$$r(\vartheta) = \sqrt{\cos^2(\vartheta) + 0.25 \sin^2(\vartheta)} = \frac{1}{2} \sqrt{1 + 3 \cos^2(\vartheta)}, \quad \vartheta \in [0, 2\pi). \quad (5.4)$$

We took the initial guess  $\mathbf{r}^0 = 1$ . The input velocity data (4.2) is numerically simulated by first solving the corresponding direct problem with  $M = 192$  and  $N = 144$ . Numerical results with or without noise and regularization are presented in Figure 6 and similar conclusions to those obtained from Figure 5 for Example 2 can be derived.

## 6. CONCLUSIONS

In this paper the MFS, which is a meshless method, has been applied for the solution of Brinkman flows in unbounded porous media exterior to known or unknown planar obstacles. For the direct well-posed linear problem when the obstacle  $\Omega$  is known, the numerically obtained results are in excellent agreement with the analytical solution, which is available when  $\Omega$  is a disk. In the inverse ill-posed and nonlinear problem, the obstacle  $\Omega$  is unknown and has to be detected from extra measurements of the fluid velocity inside the fluid domain exterior to the obstacle  $\Omega$ . In order to achieve stability, the nonlinear minimization of the gap between the measured and computed data is penalised through the inclusion of regularization parameters for the MFS expansion coefficients and for the radial function parameterising the assumed star-shaped obstacle. The MFS can also be easily implemented for three-dimensional exterior Brinkman flows. This can be accomplished by changing the two-dimensional fundamental solutions (2.1) and (2.2) to their corresponding three-dimensional expressions, [20], and using spherical instead of polar coordinates throughout the analysis. The investigation of interior Brinkman flows in a bounded porous medium around a known or unknown inclusion will be the subject of the companion Part II paper.

## ACKNOWLEDGEMENTS

The authors are grateful to the University of Cyprus for supporting this research. We would also like to thank Professor Mirela Kohr for some discussion on the infinity condition (1.12).

## REFERENCES

- [1] C. J. S. Alves and A. L. Silvestre, *Density results using Stokeslets and a method of fundamental solutions for the Stokes equations*, Eng. Anal. Boundary Elements **28** (2004), 1245–1252.
- [2] C. J. S. Alves, R. Kress and A. L. Silvestre, *Integral equations for an inverse boundary value problem for the two-dimensional Stokes equations*, J. Inverse Ill-Posed Probl. **15** (2007), 461–481.
- [3] W. Borchers and W. Varnhorn, *On the boundedness of the Stokes semigroup in two-dimensional exterior domains*, Math. Z. **213** (1993), 275–299.
- [4] H. C. Brinkman, *A calculation of the viscous force exerted by a flowing fluid in a dense swarm of particles*, Appl. Sci. Res. **1** (1949), 27–34.
- [5] L. Durlofsky and J. F. Brady, *Analysis of Brinkman equations as a model for flow in porous media*, Phys. Fluids **30** (1987), 3329–3341.
- [6] G. E. Kapellos, T. S. Alexiou and A. C. Payatakes, *Hierarchical simulator of biofilm growth and dynamics in granular porous materials*, Adv. Water Resour. **30**, 1648–1667.
- [7] A. Karageorghis and D. Lesnic, *The method of fundamental solutions for the Oseen steady-state viscous flow past obstacles of known or unknown shapes*, Numer. Methods Partial Differential Equations **35** (2019), 2103–2119.
- [8] A. Karageorghis, D. Lesnic, and L. Marin, *A survey of applications of the MFS to inverse problems*, Inverse Probl. Sci. Eng. **19** (2011), 309–336.
- [9] A. Karageorghis, D. Lesnic and L. Marin, *A moving pseudo-boundary method of fundamental solutions for void detection*, Numer. Methods Partial Differential Equations **29** (2013), 935–960.
- [10] M. Kohr, *The Dirichlet problems for the Stokes resolvent equations in bounded and exterior domain in  $\mathbb{R}^n$* , Math. Nachr. **280** (2007), 534–559.

- [11] M. Kohr, G. P. R. Sekhar and J. R. Blake, *Green's function of the Brinkman equation in a 2D anisotropic case*, IMA J. Appl. Math. **73** (2008), 374–392.
- [12] R. Kress and S. Meyer, *An inverse boundary value problem for the Oseen equation*, Math. Meth. Appl. Sci. **23** (2000), 103–120.
- [13] K. Leiderman and A. L. Fogelson, *The influence of hindered transport on the development of platelet thrombi under flow*, Bull. Math. Biol. **75** (2013), 1255–1283
- [14] K. Leiderman and S. D. Olson, *Swimming in a two-dimensional Brinkman fluid: computational modeling and regularized solutions*, Physics of Fluids **28** (2016), 021902. Erratum **29**, 029901.
- [15] I. S. Ligaarden, M. Krotkiewski, K.-A. Lie, M. Pal and D. W. Schmid, *On the Stokes-Brinkman equations for modelling flow in carbonate reservoirs*, In: Proceedings of the the ECMOR XII - 12th European Conference on the mathematics of Oil Recovery, Oxford, UK, cp-163-00006, 2010.
- [16] P. A. Martin, *Two-dimensional Brinkman flows and their relation to analogous Stokes flows*, IMA J. Appl. Math. **84** (2019), 912–929.
- [17] N. F. M. Martins and M. Rebelo, *Meshfree methods for non-homogeneous Brinkman flows*, Comput. Math. Appl. **68** (2014), 872–886.
- [18] The MathWorks, Inc., 3 Apple Hill Dr., Natick, MA, *Matlab*.
- [19] C. Pozrikidis, *Boundary Integral and Singularity Methods for Linearized Viscous Flow*, Cambridge University Press, Cambridge, 1992.
- [20] C. C. Tsai, *Solutions of slow Brinkman flows using the method of fundamental solutions*, Int. J. Numer. Methods Fluids **56** (2008), 927–940.
- [21] W. Varnhorn, *The boundary value problems of the Stokes resolvent equations in  $n$  dimensions*, Math. Nachr. **269-270** (2004), 210–230.
- [22] D. L. Young, S. J. Jane, C. M. Fan, K. Murugesan and C. C. Tsai, *The method of fundamental solutions for 2D and 3D Stokes problems*, J. Comput. Phys. **211** (2006), 1–8.

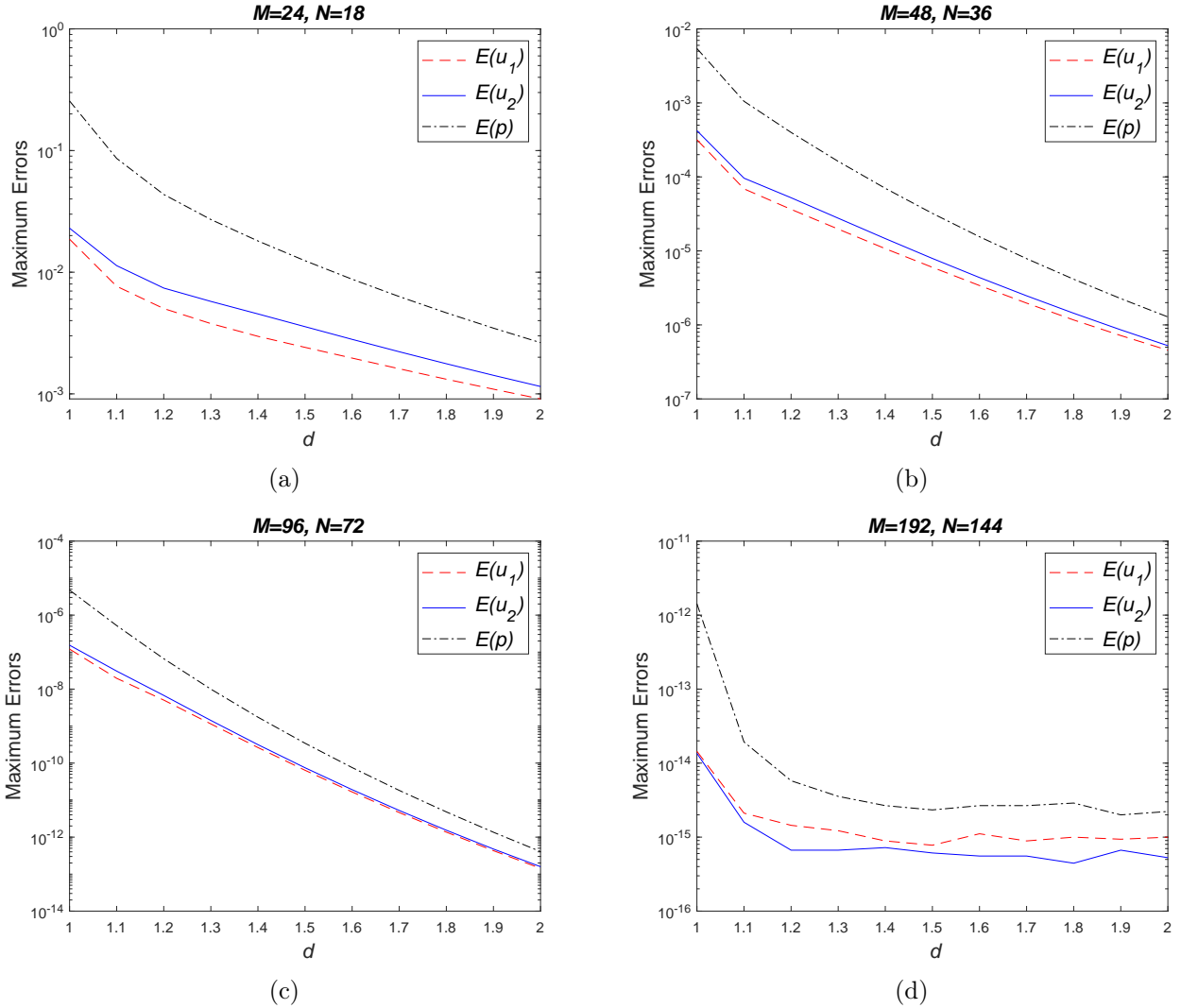


FIGURE 1. Example 1: Maximum absolute errors in perturbed velocity  $\mathbf{u} = (u_1, u_2)$  and pressure ( $E(u_1)$ ,  $E(u_2)$  and  $E(p)$ , respectively) for different numbers of degrees of freedom on circles of radii  $d$  near the boundary.

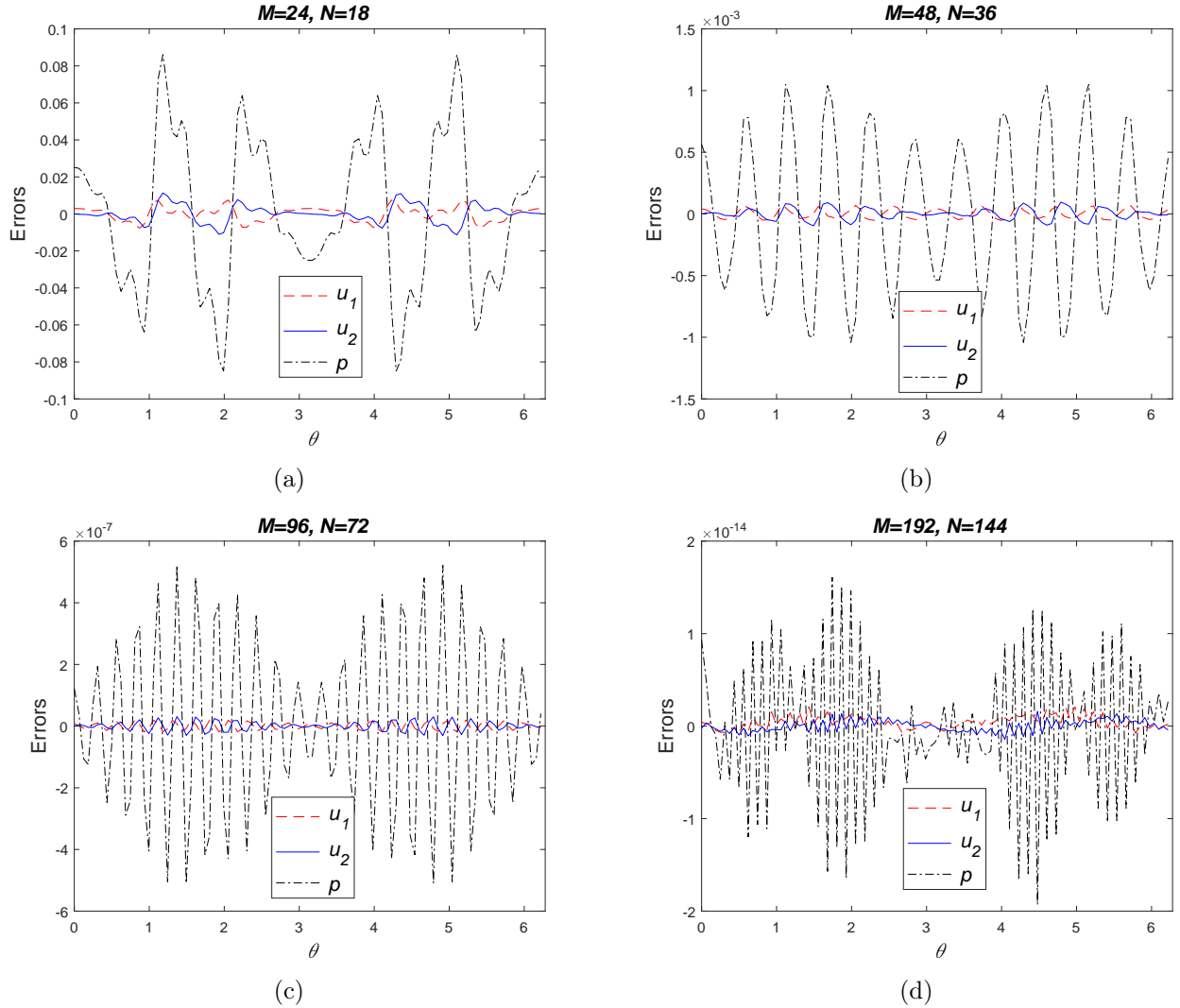


FIGURE 2. Example 1: Errors in perturbed velocity  $\mathbf{u} = (u_1, u_2)$  and pressure on the circle of radius  $d = 1.1$ .

DEPARTMENT OF MATHEMATICS AND STATISTICS, UNIVERSITY OF CYPRUS/ ΠΑΝΕΠΙΣΤΗΜΙΟ ΚΥΠΡΟΥ,  
P.O.BOX 20537, 1678 NICOSIA/ΛΕΥΚΩΣΙΑ, CYPRUS/ΚΥΠΡΟΣ  
*E-mail address:* andreask@ucy.ac.cy

DEPARTMENT OF APPLIED MATHEMATICS, UNIVERSITY OF LEEDS, LEEDS LS2 9JT, UK  
*E-mail address:* amt51d@maths.leeds.ac.uk

DEPARTMENT OF MATHEMATICS, FACULTY OF MATHEMATICS AND COMPUTER SCIENCE, UNIVERSITY OF BUCHAREST,  
14 ACADEMIEI, 010014 BUCHAREST, AND INSTITUTE OF MATHEMATICAL STATISTICS AND APPLIED MATHE-  
MATICS, ROMANIAN ACADEMY, 13 CALEA 13 SEPTEMBRIE, 050711 BUCHAREST, ROMANIA  
*E-mail address:* marin.liviu@gmail.com; liviu.marin@fmi.unibuc.ro

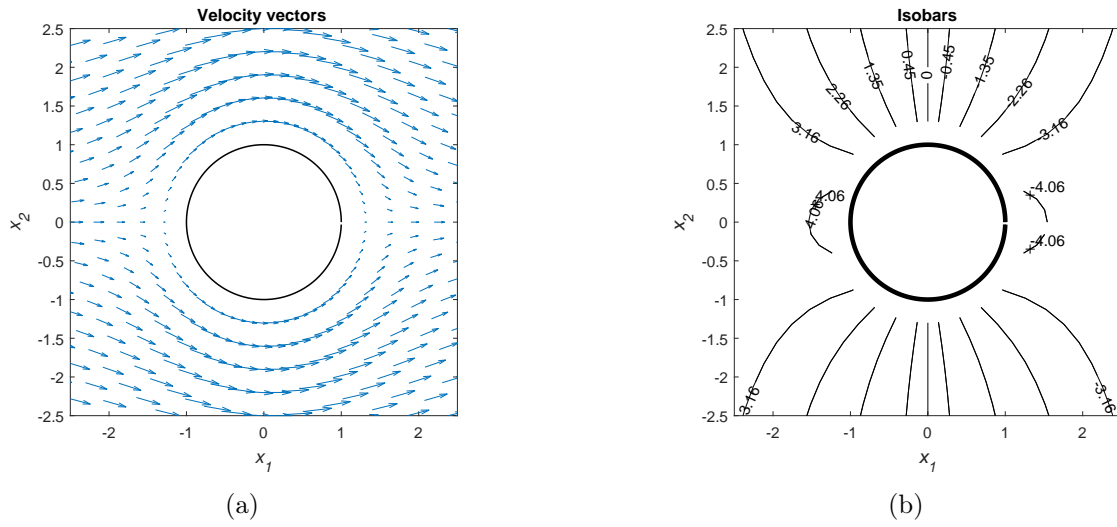


FIGURE 3. Example 1: (a) Velocity vectors (b) Lines of constant pressure (isobars).

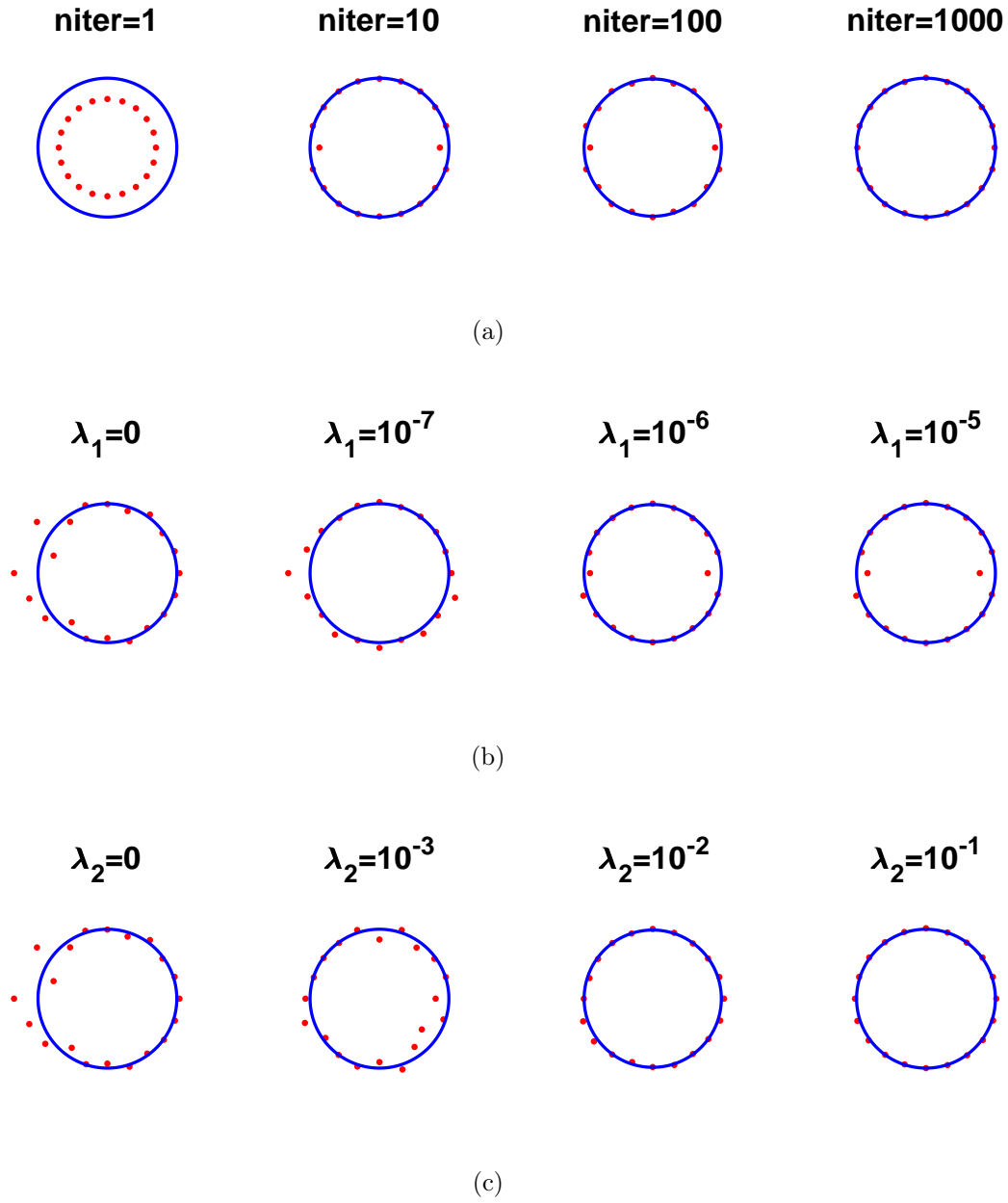


FIGURE 4. Example 1: Results (a) with no noise and no regularization, (b) for various values of  $\lambda_1$ ,  $\zeta = 5\%$  noise, and  $\lambda_2 = 0$ , (c) for various values of  $\lambda_2$ ,  $\zeta = 5\%$  noise, and  $\lambda_1 = 0$ .

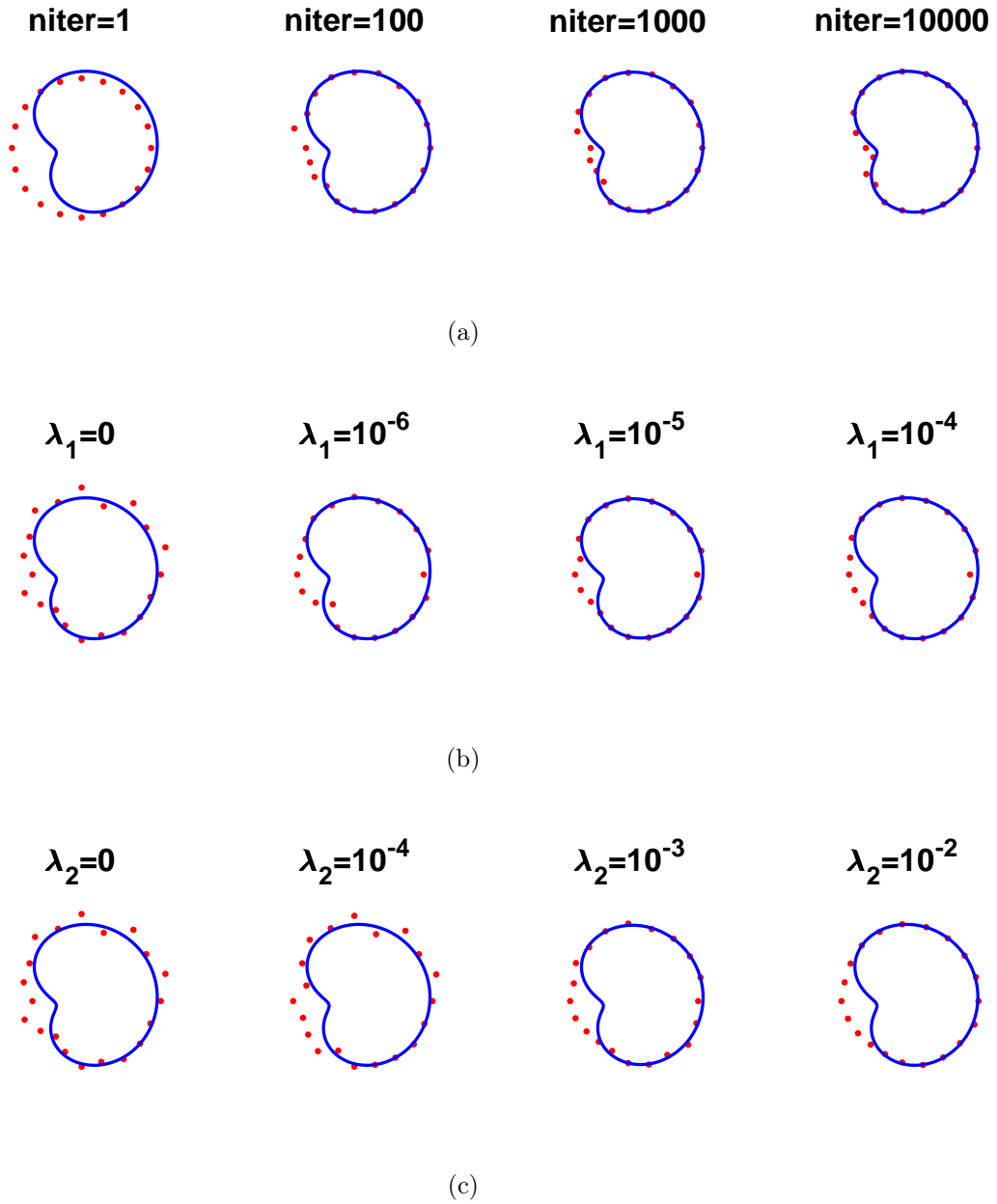


FIGURE 5. Example 2: Results (a) with no noise and no regularization, (b) for various values of  $\lambda_1$ ,  $\zeta = 5\%$  noise, and  $\lambda_2 = 0$ , (c) for various values of  $\lambda_2$ ,  $\zeta = 5\%$  noise, and  $\lambda_1 = 0$ .

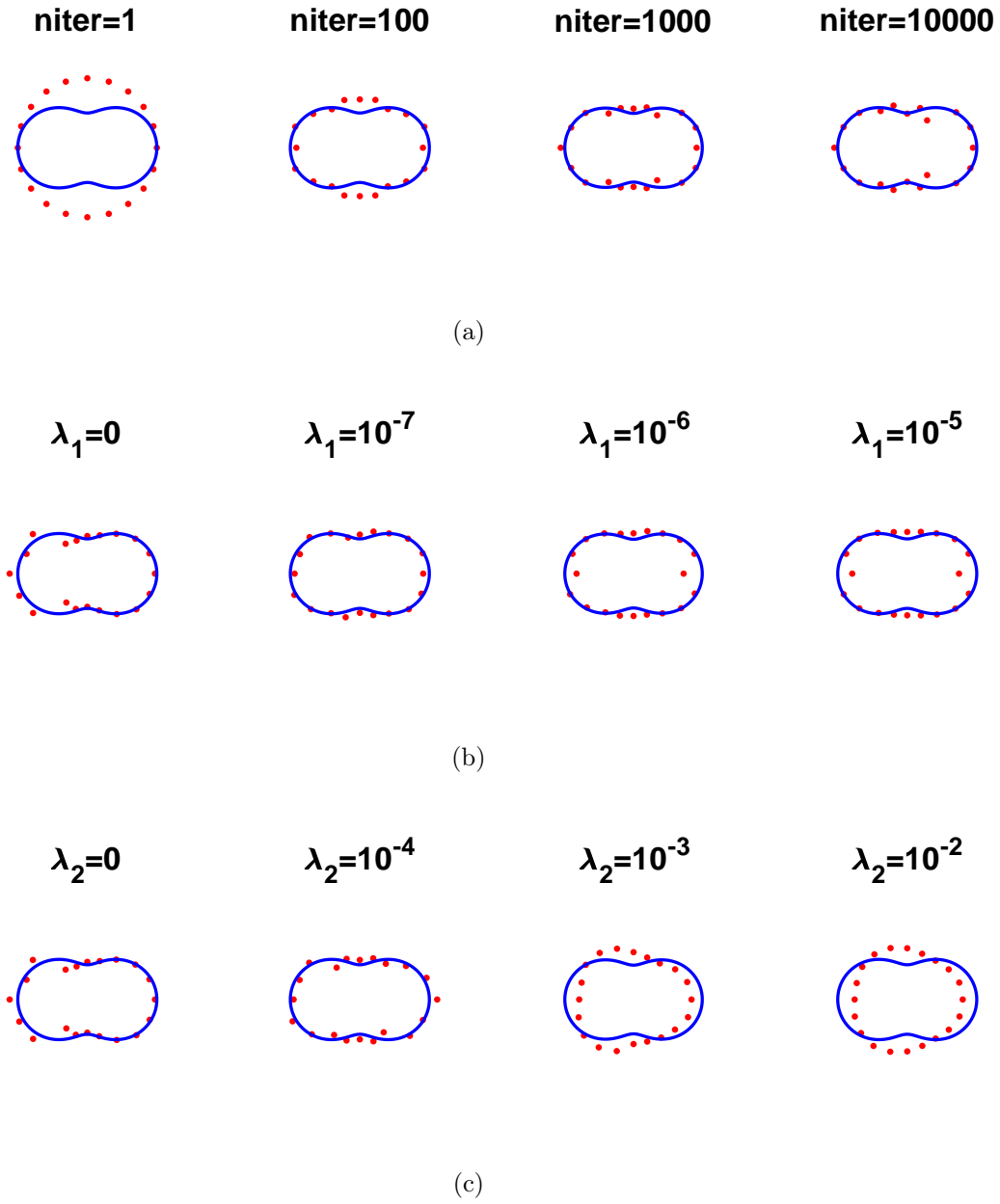


FIGURE 6. Example 3: Results (a) with no noise and no regularization, (b) for various values of  $\lambda_1$ ,  $\zeta = 5\%$  noise, and  $\lambda_2 = 0$ , (c) for various values of  $\lambda_2$ ,  $\zeta = 5\%$  noise, and  $\lambda_1 = 0$ .